





Cite this: *RSC Adv.*, 2020, 10, 31377

# Discovery of mercaptopropanamide-substituted aryl tetrazoles as new broad-spectrum metallo- $\beta$ -lactamase inhibitors†

Yu-Hang Yan, Jian Chen, Zhen Zhan, Zhu-Jun Yu, Gen Li, Li Guo, Guo-Bo Li,  Yong Wu  and Yongxiang Zheng \*

$\beta$ -Lactam antibiotic resistance mediated by metallo- $\beta$ -lactamases (MBL) has threatened global public health. There are currently no available inhibitors of MBLs for clinical use. We previously reported the ruthenium-catalyzed meta-selective C–H nitration synthesis method, leading to some *meta*-mercaptopropanamide substituted aryl tetrazoles as new potent MBL inhibitors. Here, we described the structure–activity relationship of *meta*- and *ortho*-mercaptopropanamide substituted aryl tetrazoles with clinically relevant MBLs. The resulting most potent compound **13a** showed  $IC_{50}$  values of 0.044  $\mu$ M, 0.396  $\mu$ M and 0.71  $\mu$ M against VIM-2, NDM-1 and IMP-1 MBL, respectively. Crystallographic analysis revealed that **13a** chelated to active site zinc ions *via* the thiol group and interacted with the catalytically important residues Asn233 and Tyr67, providing further structural information for the development of thiol based MBL inhibitors.

Received 23rd July 2020  
Accepted 14th August 2020

DOI: 10.1039/d0ra06405j

rsc.li/rsc-advances

## Introduction

$\beta$ -Lactam antibiotics remain the most important class of antibiotics due to their safety, high efficacy and broad-spectrum antibacterial activity.<sup>1</sup> The emergence and rapid worldwide distribution of  $\beta$ -lactam-resistant bacteria pathogens poses an increasing clinical threat to human health and life.<sup>2–4</sup>  $\beta$ -Lactam hydrolysis mediated by  $\beta$ -lactamase is a major contributor to the resistance in bacteria.<sup>5,6</sup> Based on different catalytic mechanisms,  $\beta$ -lactamases are categorized into two groups: serine  $\beta$ -lactamases (SBLs) and metallo- $\beta$ -lactamases (MBLs).<sup>5</sup> SBLs employ an active-site nucleophilic serine to hydrolyze the  $\beta$ -lactam ring, while MBLs utilize a Zn(II)-bound hydroxyl group to achieve nucleophilic attack on the  $\beta$ -lactam carbonyl, ultimately leading to the cleavage of the  $\beta$ -lactam ring.<sup>7,8</sup> Several SBL inhibitors, such as clavulanic acid, tazobactam, sulbactam, avibactam, and vaborbactam, have been successfully applied in combination with beta-lactam antibiotics to treat infections caused by SBL-producing bacteria in clinics.<sup>9,10</sup> However, there are no FDA-approved MBL inhibitors.<sup>11,12</sup>

On the basis of sequence and structural similarities, MBL enzymes can be divided into three subclasses (B1, B2, B3).<sup>7</sup>

Subclass B1 MBLs contain the most clinically significant types, such as the New Delhi MBL (NDMs), imipenemase (IMPs), and Verona integron-encoded MBL (VIMs), representing the major targets for developing inhibitors with therapeutic value.<sup>13</sup> So far, various types of MBL inhibitors have been reported, such as thiol-containing compounds, cyclic boronates, succinic acids, carboxylates and others.<sup>14–20</sup> Most MBL inhibitors work *via* active-site metal chelation manner, and more importantly, the broad-spectrum MBL inhibitors have metal chelation and anchor residue binding features.<sup>14</sup> Despite progress has been made, there is still a need to develop new broad-spectrum MBL inhibitors to provide candidates for the development of clinically useful MBL inhibitors.

In our previous study, we described a new synthesis method, namely ruthenium-catalyzed meta-selective C–H nitration, which led to new potent MBL inhibitors; these inhibitors contain an aryl tetrazole fragment and a mercaptopropanamide moiety as the metal binding pharmacophore.<sup>21</sup> This work presents structure–activity relationship (SAR) studies of mercaptopropanamide substituted aryl tetrazoles with clinically relevant MBLs and crystallographic analyses of the mechanism-of-inhibition of this chemotype inhibitors. We synthesized a series of *ortho*- and *meta*-mercaptopropanamide substituted aryl tetrazole derivatives through C–H activation methods, and tested for their inhibitory activity against three MBL enzymes, including VIM-2, NDM-1 and IMP-1. Among all the synthesized target compounds, *meta*-mercaptopropanamide substituted aryl tetrazole **13a** had the strongest inhibitory activity against clinically relevant VIM-2, NDM-1 and IMP-1 with  $IC_{50}$  values of 0.044  $\mu$ M, 0.396  $\mu$ M

Key Laboratory of Drug Targeting and Drug Delivery System of Ministry of Education, Sichuan Engineering Laboratory for Plant-Sourced Drug, Sichuan Research Center for Drug Precision Industrial Technology, West China School of Pharmacy, Sichuan University, Sichuan 610041, China. E-mail: yongxiangzheng@scu.edu.cn; Tel: +86 199 3880 2868

† Electronic supplementary information (ESI) available. See DOI: 10.1039/d0ra06405j



and 0.71  $\mu\text{M}$ , respectively. Crystallographic analyses showed that **13a** chelated to both active site zinc ions *via* thiol group and interacted with catalytically important residues on the L1 and L3 loop.

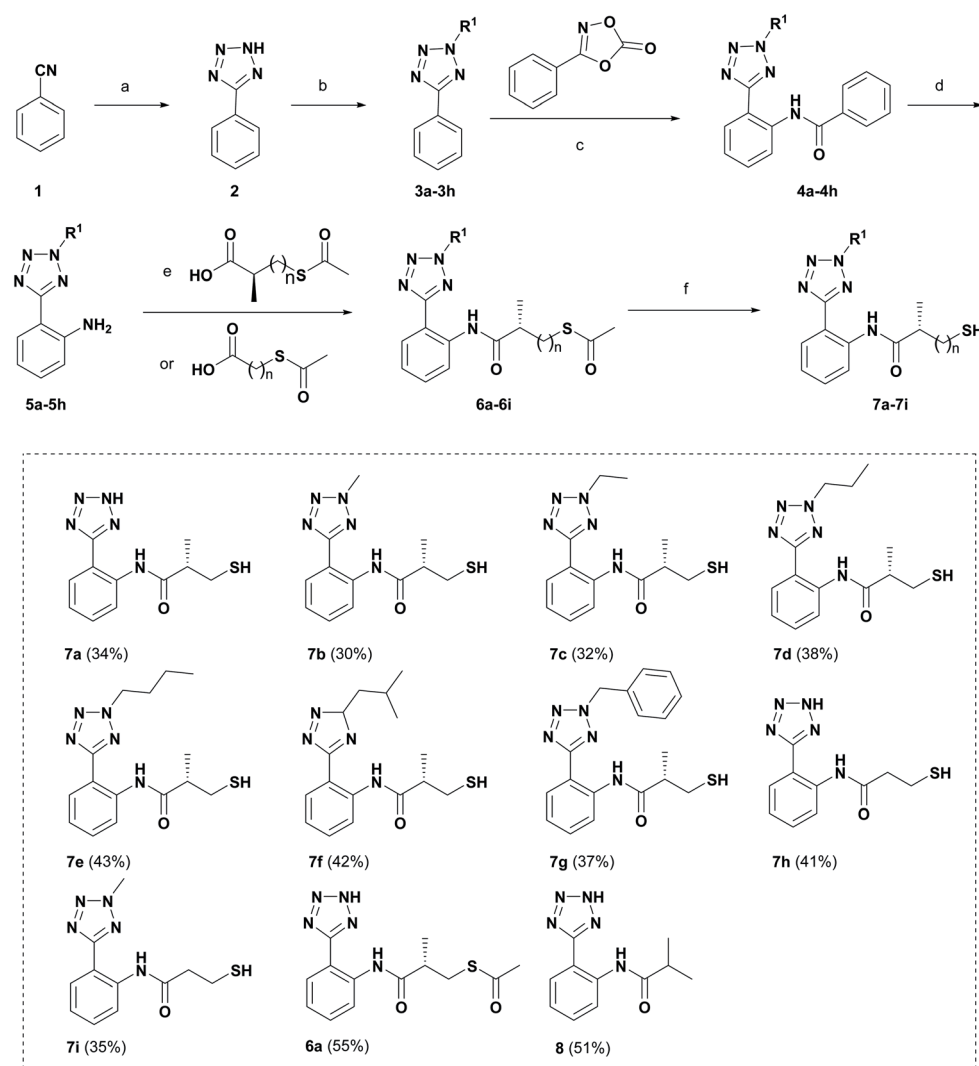
## Results and discussion

### Chemistry

Schemes 1 and 2 show the synthetic routes and total yields of all target compounds. Compounds **6a**, **7a–7i** and **8** were synthesized using the reaction sequence shown in Scheme 1. Compound **2** was obtained by using benzonitrile to react with  $\text{NaN}_3$  in the presence of  $\text{ZnBr}_2$  and  $\text{H}_2\text{O}$  stirring at 100  $^\circ\text{C}$  for 24 h.<sup>22</sup> Compounds **3a–3h** were synthesized by the reactions of compound **2** and different iodoalkanes.<sup>23</sup> Then, compounds **3a–3h** were reacted with 3-phenyloxazolidinone to afford the corresponding amides **4a–4h** *via* the C–H activation strategy as described previously, followed by reacting with sodium

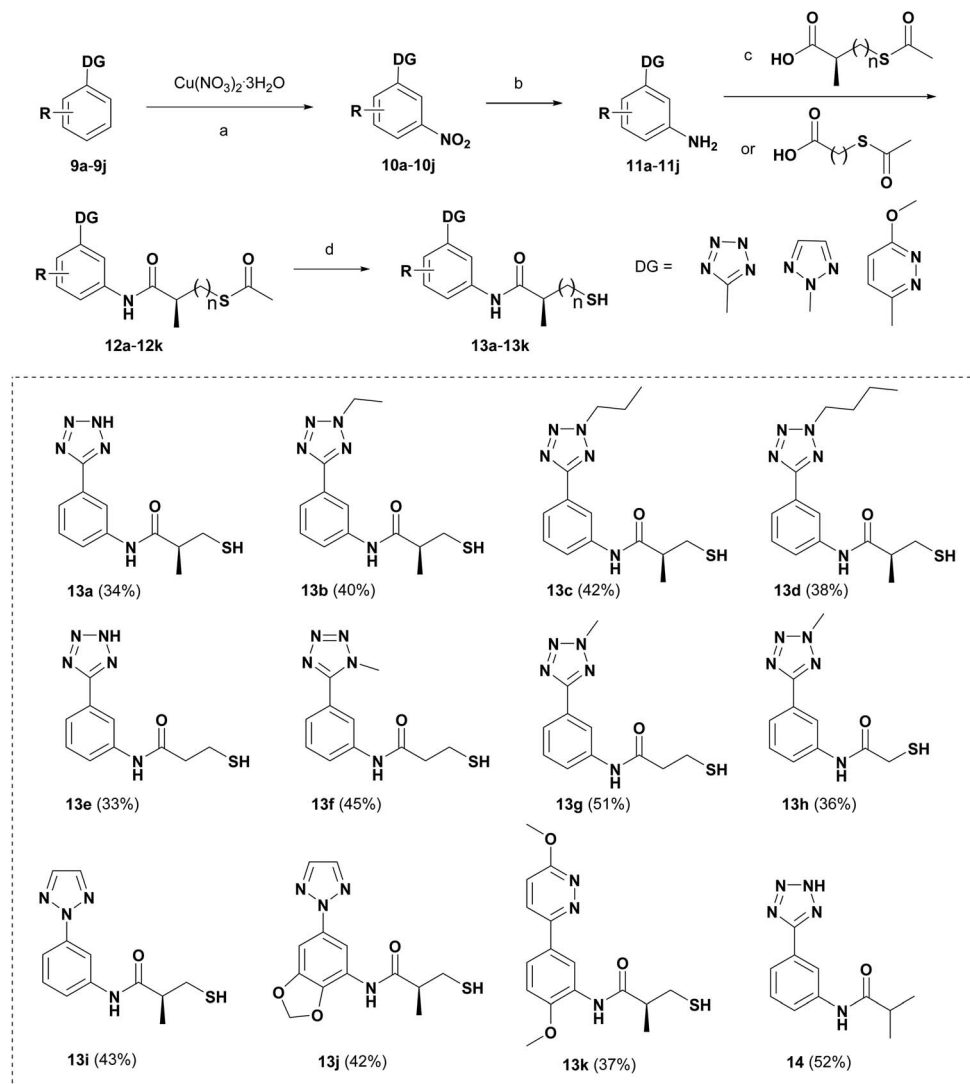
hydroxide to produce 2-(2H-tetrazol-5-yl)anilines (**5a–5h**).<sup>21</sup> Subsequently, Compounds **5a–5h** were treated with different carboxylic acids, giving the thioesters (**6a–6i**) in high yields. Finally, the desired compounds **7a–7i** were furnished through the hydrolysis reactions of **6a–6i** in the presence of  $\text{NH}_3 \cdot \text{H}_2\text{O}$  under argon atmosphere. Compound **5a** was subjected to the condensation reaction by isobutyryl chloride to give the desired compound **8**.

Scheme 2 shows the synthetic route for target compounds **12a**, **13a–13k** and **14**. Compounds **9a–9j** were reacted with  $\text{Cu}(\text{NO}_3)_2 \cdot 3\text{H}_2\text{O}$  to afford the *meta*-nitrated products **10a–10j** *via* the C–H activation strategy, followed by the reduction reactions to give the compounds **11a–11j**.<sup>24</sup> Then, the thioesters **12a–12k** were readily synthesized by the condensation reactions of **11a–11j** with different carboxylic acids. Subsequently, the hydrolysis reactions of **12a–12k** produced the target compounds **13a–13k**. Compound **14** was obtained by the condensation reaction of compound **9a** and isobutyryl chloride.



**Scheme 1** Preparation of target compounds **7a–7i**, **6a** and **8**. Reagents and conditions: (a)  $\text{NaN}_3$ ,  $\text{ZnBr}_2$ ,  $\text{H}_2\text{O}$ , reflux, 24 h; (b)  $\text{K}_2\text{CO}_3$ , rt, 5 min;  $\text{R}^1$ –I, 85  $^\circ\text{C}$ , 4 h; (c)  $[\text{Cp}^*\text{RhCl}_2]_2$ ,  $\text{Ag}_2\text{SO}_4$ , DCE, 80  $^\circ\text{C}$ , 24 h; (d)  $\text{NaOH}$ ,  $\text{EtOH}$ , reflux, 1 h; (e) IBCF, NMM, dry DCM, rt, 24 h; (f)  $\text{NH}_3 \cdot \text{H}_2\text{O}$ , Ar, rt, 2 h. The overall yield for each target compound is shown in brackets behind the compound number.





Scheme 2 Preparation of target compounds **13a–13k** and **14**. Reagents and conditions: (a)  $\text{Ru}_3(\text{CO})_{12}$ ,  $\text{PPh}_3$ ,  $\text{PhI}(\text{TFA})_2$ , HFIP,  $100^\circ\text{C}$ , 24 h; (b)  $\text{H}_2$ , 10% Pd/C, MeOH; (c) IBCF, NMM, dry DCM, rt, 24 h; (d)  $\text{NH}_3 \cdot \text{H}_2\text{O}$ , Ar, rt, 2 h.

### SAR of mercaptopropionamide substituted aryl tetrazole derivatives with MBLs

We evaluated the inhibitory activity of all the targeted compounds against clinically important VIM-2, NDM-1 and IMP-1 by using a fluorescence-based assay (Fig. S1†).<sup>25</sup> As shown in Table 1, **7a–7g** contain mercapto-2-methylpropanamide substituents on the *ortho* position of the phenyl ring. **7a** displayed potent inhibition on VIM-2 with  $\text{IC}_{50}$  value of  $0.035\ \mu\text{M}$  and moderate inhibition on NDM-1 and IMP-1. Addition of alkyl or benzyl substituents to the N-2 of tetrazole of **7a** slightly decreased the inhibitory activity of VIM-2, but increased the inhibitory activity on NDM-1 and IMP-1, except for **7b** with methyl substitution on the tetrazole, which showed less potent inhibition against all the tested enzymes, especially for NDM-1. The *ortho*-mercaptopropionamide-substituted derivatives **7h** and **7i** showed comparable inhibition with **7a**. Comparison of **7a**, **7h**, and **7i** indicated that the effect of methyl substitution on the tetrazole of **7h** on the activity of NDM-1 was not as great as

that of **7a**, which was reduced by about 5 times. Two examples showed that the thiol group was important for interacting with the active site: (1) the product **6a** with acetylation modification on the thiol group exhibited significantly reduced inhibitory activity; (2) no inhibition against tested MBL enzymes was observed for **8** without the thiol group.

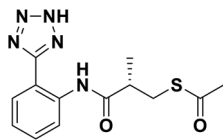
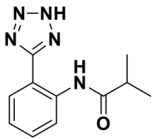
Then, we investigated the activity of compounds with mercaptopropionamide substitutions on the *meta* position of the phenyl ring (Table 2, Fig. S1†). Among all the synthesized mercaptopropionamide derivatives, **13a** manifested the most potent inhibition, displaying  $\text{IC}_{50}$  values of  $0.044\ \mu\text{M}$ ,  $0.396\ \mu\text{M}$  and  $0.71\ \mu\text{M}$  against VIM-2, NDM-1 and IMP-1, respectively. Introduction of alkane chain on the 2-N of tetrazole resulted in **13b–13d**. Compared to **13a**, **13b–13d** exhibited compared inhibition on VIM-2 and decreased inhibition on NDM-1 and IMP-1. Mercaptopropionamide substituted compound **13e** showed  $\text{IC}_{50}$  values of  $0.021\ \mu\text{M}$ ,  $6.10\ \mu\text{M}$  and  $0.44\ \mu\text{M}$  against VIM-2, NDM-1 and IMP-1, respectively, indicating that the methyl

Table 1 Inhibitory activities of *ortho*-mercaptopropanamide substituted aryl tetrazole derivatives against representative MBL enzymes

Cpds	Chemical structure	IC <sub>50</sub> value (μM)/pIC <sub>50</sub> /s.e. pIC <sub>50</sub>		
		VIM-2	NDM-1	IMP-1
7a		0.035/7.45/0.039	10.75/4.97/0.046	9.87/5.01/0.118
7b		1.82/5.74/0.050	>100/—/—	12.26/4.90/0.127
7c		0.06/7.22/0.050	1.84/5.74/0.048	0.13/6.89/0.107
7d		0.49/6.37/0.024	0.83/6.08/0.138	0.88/6.056/0.057
7e		0.16/6.81/0.062	2.0/5.69/0.056	1.49/5.83/0.084
7f		1.70/5.77/0.039	2.59/5.59/0.076	1.34/5.87/0.099
7g		0.16/6.81/0.047	1.46/5.84/0.036	1.36/5.87/0.043
7h		0.028/7.55/0.044	3.16/5.50/0.041	10.17/4.99/0.076
7i		0.026/7.59/0.033	19.52/4.70/0.094	4.68/5.33/0.166



Table 1 (Contd.)

Cpds	Chemical structure	IC <sub>50</sub> value (μM)/pIC <sub>50</sub> /s.e. pIC <sub>50</sub>		
		VIM-2	NDM-1	IMP-1
6a		0.63/6.20/0.049	30.16/4.52/0.077	30.41/4.52/0.088
8		>100/—/—	>100/—/—	>100/—/—

substitution on the  $\alpha$ -C of the carbonyl group had a great influence on the activity of NDM-1. For the methyl substituted on N-1 or N-2 of **13e** derivatives **13f** and **13g**, no significant impact of the substitution position on NDM-1 and IMP-1 inhibition was found, but methyl substitution on N-1 was unfavorable for VIM-2 activity. In addition, the shortening of the alkyl chain was also adverse to the inhibition on VIM-2, as exemplified by **13h**. Furthermore, we also explored the effect of different heterocycles-replacing biphenyltetrazole (**13i–13k**) on MBL inhibitory activity. Obviously, substitution of aromatic ring had the greatest effect on NDM-1 and IMP-1 inhibition, which led to at least 3-fold drop in activity. The activity of **13i–13k** on VIM-2 was comparable to or slightly weaker than that of **13a**. Similar to what was observed before, **14** without thiol group had very low inhibitory activity on tested MBLs.

Moreover, we assessed the effect of the most potent inhibitor **13a** on a cellular level through minimum inhibitory concentrations (MIC) assay (Table S2†). The results indicated that **13a** potentiated the efficacy of meropenem at 100 μM against laboratory-constructed VIM-2 expressing *E. coli* strain with MIC value of 4 μg mL<sup>-1</sup>.

### Crystallographic analysis

In order to investigate the binding mode of the most potent compound **13a**, we obtained the X-ray structure of VIM-2 in complex with **13a** by co-crystal experiments. The VIM-2: **13a** (PDB ID 7CJL) complex structure was solved to 1.79 Å resolution (Table S1†). The VIM-2:**13a** complex crystallized in a P 212121 space group with two molecules in the asymmetric unit (ASU) and was refined to  $R_{\text{work}}/R_{\text{free}}$  value of 20.53/24.64% (Table S1†). The crystal structure revealed that **13a** was positioned to bridge two active site zinc ions replacing the nucleophilic water the thiol group, which was common for the binding of thiol-containing MBL inhibitors with VIM-2 (Fig. 1).<sup>15,17,19</sup> And the carbonyl group makes hydrogen-bonding interactions with catalytically important residue Asn233 on the L3 loop. In addition, the phenyl group forms face-to-face  $\pi$ - $\pi$  interactions with Tyr67 on the L1 loop. Although **13a** did not have negatively

charged group to interact with the positively charged residue Arg228, it manifested potent MBL inhibition *via* specific binding with the flexible L1 loop, which provide new insights into inhibitor design of MBL inhibitors.

## Conclusions

In conclusion, a series of mercaptopropionamide-substituted aryl tetrazole derivatives were synthesized *via* the C–H activation strategy, which will provide new strategies to readily derive new *meta*- and *ortho*-substituted aryl tetrazoles or other related derivatives. The SAR studies of these synthesized derivatives with three representative MBL enzymes led to the identification of **13a** as a potent, broad-spectrum MBL inhibitor with IC<sub>50</sub> values of 0.044 μM, 0.396 μM and 0.71 μM against VIM-2, NDM-1 and IMP-1, respectively. The crystal structure of VIM-2 in complex with **13a** revealed that **13a** was positioned to bridge the active site zinc ions *via* the thiol group and interacted with catalytically important residues on the L1 and L3 loop. Notably, **13a** was observed to fit well with the flexible L1 loop, providing new insights for further development of potent MBL inhibitors of clinical relevance.

## Experimental

### Protein expression and purification

VIM-2 (27–266 aa), NDM-1 (1–270 aa) and IMP-1 (19–246 aa) were expressed and purified as previously published procedures.<sup>15</sup>

### Inhibition assays

The experiments were carried out by using Tecan microplate reader and flat-bottom 96-well black plates at room temperature. Compounds were dissolved into 100 mM with DMSO. All the MBL enzymes were dissolved in the assay buffer: 20 mM Tris-HCl (pH 7.5), 200 mM NaCl. The compounds (with 10 different concentrations in 3-fold dilution) pre-incubated with appropriate amount of MBL enzymes for 10 min. The reactions were initiated by adding of the substrate FC5. The IC<sub>50</sub> values



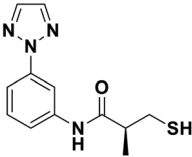
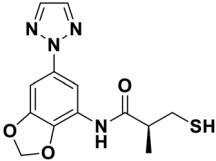
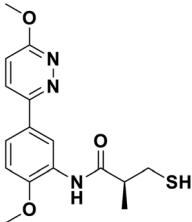
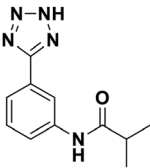
Table 2 Inhibitory activities of *meta*-mercaptopropanamide substituted benzoheterocycle derivatives against representative MBL enzymes

Cpds	Chemical structure	IC <sub>50</sub> value (μM)/pIC <sub>50</sub> /s.e. pIC <sub>50</sub>		
		VIM-2	NDM-1	IMP-1
13a		0.044/7.35/0.022	0.396/6.40/0.036	0.71/6.15/0.089
13b		0.082/7.08/0.026	3.02/5.52/0.032	6.23/5.21/0.153
13c		0.018/7.74/0.039	2.37/5.63/0.040	1.23/5.91/0.050
13d		0.025/7.60/0.066	2.65/5.58/0.030	4.97/5.30/0.384
13e		0.021/7.67/0.038	6.10/5.21/0.028	0.44/6.30/0.192
13f		0.48/6.32/0.056	3.23/5.49/0.023	1.54/5.81/0.106
13g		0.079/7.10/0.040	4.19/5.38/0.065	1.18/5.93/0.067
13h		1.38/5.86/0.091	3.22/5.49/0.024	0.94/6.03/0.053





Table 2 (Contd.)

Cpds	Chemical structure	IC <sub>50</sub> value (μM)/pIC <sub>50</sub> /s.e. pIC <sub>50</sub>		
		VIM-2	NDM-1	IMP-1
13i		0.11/6.97/0.036	2.10/5.68/0.048	3.70/5.43/0.062
13j		0.025/7.60/0.034	1.27/5.90/0.058	4.19/5.38/0.399
13k		0.056/7.25/0.041	1.27/5.90/0.067	1.56/5.81/0.199
14		>100/—/—	>100/—/—	>100/—/—

for the compounds were determined by monitoring the fluorescence at  $\lambda_{\text{ex}}$  of 380 nm and  $\lambda_{\text{em}}$  of 460 nm. All determinations were tested in triplicate. The IC<sub>50</sub> values were fitted by using GraphPad Prism5 software.

#### Microdilution broth minimum inhibitory concentrations (MICs) assay

Strains of *E. coli* DH5a containing plasmids pET28-lacUV5-VIM-2 (*E. coli*-VIM-2) and pET28-lacUV5 (as control) were used to assess the inhibitors.<sup>17</sup> Single colonies of the *E. coli*-VIM-2 strain on MH agar plates were transferred to 5 mL of MH liquid medium, and grown at 37 °C to an OD<sub>630</sub> of ~0.5. The concentrations of *E. coli*-VIM-2 and *E. coli* strains were diluted to ~10<sup>6</sup> colony forming units (CFU) per mL in the MH medium, then transferred to the microtiter plates, and treated with meropenem (final concentrations of 128 mg mL<sup>-1</sup> to 0.25 mg mL<sup>-1</sup> in 2-fold dilution) or/and the inhibitors **13a** (final concentrations of 25–200 μM, 2-fold concentration gradient). The microtiter plates were incubated for 16–20 h at 37 °C and visually evaluated for bacterial growth. Each determinate was performed in duplicate.

#### Crystallization and data collection

X-ray structure of VIM-2 in complex with inhibitors **13a** was obtained as previously described. Briefly, the mixture of 10 mg mL<sup>-1</sup> VIM-2 protein and 5 mM inhibitor was incubated in crystallization buffer (20 mM Tris-HCl, pH 7.5, 200 mM NaCl, 0.5 mM tris(2-carboxyethyl)phosphine (TCEP)) for 60 min at

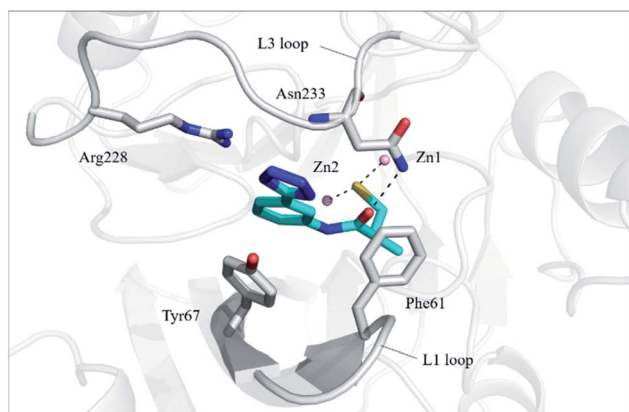


**Fig. 1** Crystallographic analyses reveal the binding modes of **13a** to VIM-2. The active-site zinc ions are shown as pink spheres. The key residues and **13a** are shown as sticks. View from crystal structures of VIM-2 in complex with **13a** (PDB ID 7CJL) reveal that the inhibitor binds to chelate with active site zinc ions and form interactions with residues on the L1 and L3 loops.



4 °C. The crystallization drops constituted of a 1 : 1 ratio of protein-inhibitor mixture : reservoir solutions (25–32% PEG 3350, 0.2 M magnesium formate). The crystals were cryo-protected using a solution of 30% (v/v) glycerol, and flash-cooled in liquid nitrogen. Data were collected at the Shanghai Synchrotron Radiation Facility, and processed using HKL2000 (Otinowski and Minor, 1997). The molecular replacement and refinement were carried out by using Phenix and Wincoot.<sup>15</sup>

## Conflicts of interest

There are no conflicts to declare.

## Acknowledgements

The authors thank the financial support from the National Natural Science Foundation (81874291), Sichuan Science and Technology Program (2018HH0100), and Outstanding Interdiscipline Project of West China Hospital of Sichuan University (grant no: ZYJC18024).

## Notes and references

- 1 T. P. Van Boeckel, S. Gandra, A. Ashok, Q. Caudron, B. T. Grenfell, S. A. Levin and R. Laxminarayan, *Lancet Infect. Dis.*, 2014, **14**, 742–750.
- 2 K. Garber, *Nat. Rev. Drug Discovery*, 2015, **14**, 445–447.
- 3 D. Brown, *Nat. Rev. Drug Discovery*, 2015, **14**, 821–832.
- 4 K. Bush, P. Courvalin, G. Dantas, J. Davies, B. Eisenstein, P. Huovinen, G. A. Jacoby, R. Kishony, B. N. Kreiswirth, E. Kutter, S. A. Lerner, S. Levy, K. Lewis, O. Lomovskaya, J. H. Miller, S. Mobashery, L. J. V. Piddock, S. Projan, C. M. Thomas, A. Tomasz, P. M. Tulkens, T. R. Walsh, J. D. Watson, J. Witkowski, W. Witte, G. Wright, P. Yeh and H. I. Zgurskaya, *Nat. Rev. Microbiol.*, 2011, **9**, 894–896.
- 5 K. Bush and G. A. Jacoby, *Antimicrob. Agents Chemother.*, 2010, **54**, 969–976.
- 6 M. W. Crowder, J. Spencer and A. J. Vila, *Acc. Chem. Res.*, 2006, **39**, 721–728.
- 7 M.-N. Lisa, A. R. Palacios, M. Aitha, M. M. González, D. M. Moreno, M. W. Crowder, R. A. Bonomo, J. Spencer, D. L. Tierney, L. I. Llarrull and A. J. Vila, *Nat. Commun.*, 2017, **8**, 538.
- 8 J. Brem, R. Cain, S. Cahill, M. A. McDonough, I. J. Clifton, J.-C. Jiménez-Castellanos, M. B. Avison, J. Spencer, C. W. G. Fishwick and C. J. Schofield, *Nat. Commun.*, 2016, **7**, 12406–12413.
- 9 D. Y. Wang, M. I. Abboud, M. S. Markoulides, J. Brem and C. J. Schofield, *Future Med. Chem.*, 2016, **8**, 1063–1084.
- 10 K. A. Toussaint and J. C. Gallagher, *Ann. Pharmacother.*, 2015, **49**, 86–98.
- 11 K. Bush and P. A. Bradford, *Nat. Rev. Microbiol.*, 2019, **17**, 295–306.
- 12 A. Krajnc, J. Brem, P. Hinchliffe, K. Calvopina, T. D. Panduwawala, P. A. Lang, J. Kamps, J. M. Tyrrell, E. Widlake, B. G. Saward, T. R. Walsh, J. Spencer and C. J. Schofield, *J. Med. Chem.*, 2019, **62**, 8544–8556.
- 13 R. R. Watkins and R. A. Bonomo, *Expert Rev. Anti-Infect. Ther.*, 2013, **11**, 543–545.
- 14 Y. H. Yan, G. Li and G. B. Li, *Med. Res. Rev.*, 2020, **40**(5), 1558–1592.
- 15 Y. L. Wang, S. Liu, Z. J. Yu, Y. Lei, M. Y. Huang, Y. H. Yan, Q. Ma, Y. Zheng, H. Deng, Y. Sun, C. Wu, Y. Yu, Q. Chen, Z. Wang, Y. Wu and G. B. Li, *J. Med. Chem.*, 2019, **62**, 7160–7184.
- 16 Z. J. Yu, S. Liu, S. Zhou, H. Li, F. Yang, L. L. Yang, Y. Wu, L. Guo and G. B. Li, *Bioorg. Med. Chem. Lett.*, 2018, **28**, 1037–1042.
- 17 S. Liu, L. Jing, Z. J. Yu, C. Wu, Y. Zheng, E. Zhang, Q. Chen, Y. Yu, L. Guo, Y. Wu and G. B. Li, *Eur. J. Med. Chem.*, 2018, **145**, 649–660.
- 18 C. Zhang, Y.-c. Pu, Z.-J. Yu, C.-y. Wu, J. Brem, M. A. McDonough, C. J. Schofield, G.-B. Li and Y. Wu, *Org. Chem. Front.*, 2018, **5**, 1288–1292.
- 19 G. B. Li, J. Brem, R. Lesniak, M. I. Abboud, C. T. Lohans, I. J. Clifton, S. Y. Yang, J. C. Jimenez-Castellanos, M. B. Avison, J. Spencer, M. A. McDonough and C. J. Schofield, *Chem. Commun.*, 2017, **53**, 5806–5809.
- 20 G.-B. Li, M. I. Abboud, J. Brem, H. Someya, C. T. Lohans, S.-Y. Yang, J. Spencer, D. W. Wareham, M. A. McDonough and C. J. Schofield, *Chem. Sci.*, 2017, **8**, 928–937.
- 21 J. Chen, T. Huang, X. Gong, Z. J. Yu, Y. Shi, Y. H. Yan, Y. Zheng, X. Liu, G. B. Li and Y. Wu, *Adv. Synth. Catal.*, 2020, **362**(14), 2984–2989.
- 22 L. Wang, W. Wu, Q. Chen and M. He, *Org. Biomol. Chem.*, 2014, **12**, 7923–7926.
- 23 C. S. Chang, Y. T. Lin, S. R. Shih, C. C. Lee, Y. C. Lee, C. L. Tai, S. N. Tseng and J. H. Chern, *J. Med. Chem.*, 2005, **48**, 3522–3535.
- 24 S. C. Kohler, S. Vahdati, M. S. Scholz and M. Wiese, *Eur. J. Med. Chem.*, 2018, **146**, 483–500.
- 25 S. S. van Berkel, J. Brem, A. M. Rydzik, R. Salimraj, R. Cain, A. Verma, R. J. Owens, C. W. Fishwick, J. Spencer and C. J. Schofield, *J. Med. Chem.*, 2013, **56**, 6945–6953.

